Effect of artificial snowing system on the stability of a ski slope in the Dolomites

Francesca Ceccato, Simonetta Cola, Veronica Girardi & Paolo Simonini
DICEA - University of Padua, Italy

francesca.ceccato@dicea.unipd.it

Abstract

In a Spring day of 2006, early afternoon, the Cianross ski slope, located in the Dolomitic skiing area in the village of San Vigilio di Marebbe (Italy) collapsed and moved slowly downwards. Due to this phenomenon, the uphill station and upper pier of a new cableway crossing the ski slope tilted and moved tens of meters down the slope scaring the people of the village and the authorities. The sliding mass, consisting of a mixture of sandstone boulders and remoulded soil permeated by an exceptionally high content of water, stopped at the lower station of the cableway, partially submerging the station itself. The investigations carried out after the collapse provided an insight of the sliding movement together with the measurement of relevant mechanical properties of the soils forming the slope. This geological and geotechnical characterization together with the geometric information of the collapsed mass allowed to tentatively perform numerical simulation of the landslide with the Material Point Method (MPM), that seems to be a powerful tool to properly describe the run-out of the sliding mass. The paper presents and discuss the case history as well as the main results and MPM modelling of the ski slope failure and propagation.

1 INTRODUCTION

On April, 22th 2006, early afternoon, a snow-capped ski slope, named Cianross and located in the worldwide known Dolomitic skiing area, collapsed moving towards the village of San Vigilio di Marebbe (Italy). Due to the landslide, the uphill station and upper pier of a new cableway crossing the ski slope tilted and moved tens of meters down the slope, finally stopping close to San Vigilio village and partially submerging the lower station of the cableway. Figure 1 shows a satellite view of the ski slope facing the village, before and after the occurrence of the flow slide. According to the slope inclination, the path of the soil mass started in South-East direction to flow then to the East direction impacting the lower station.

The fluidized soil volume consisted of a mixture of sandstone boulders and remoulded material derived from strongly decomposed sandstone rocks with an exceptionally high content of water. The visual inspection of the slope a few hours after the event showed that a pipe of the snow-making system crossing the crest of the landslide at small depth had been cut off.

The catastrophic event was caused by an unfavourable combination of different factors. It seemed that the onset of failure was located along pre-existing subsoil weakness planes of a quiescent pre-existing small landslide. This was due to the relevant amount of vertical water percolation as a consequence of snow melting as well as to seepage in the slope in springtime. These small movements cut off the pipe system supplying water at very high pressure to the snow guns in the area. The additional water flow at very high outflow rate led to an additional extremely relevant water supply, which increased the water pressure reducing the frictional resistance and increasing the downhill stress components. When the movement got started, the water saturated soil volume liquefied and flowed down the slope.

Computational modelling of such type of landslide should include the onset of failure and the response in subsequent times describing the motion of the sliding mass. The transition from stable to fluidized condition involves relevant soil-water interactions and large displacements. As a result of that, the evolution of the slope collapse becomes a very complex phenomenon. The classical limit equilibrium methods and finite element methods have been used in many studies to predict the failure mechanisms in slope stability evaluation, but they are not suitable to describe post failure responses (i.e. the run-out) due to their limitations in modelling large displacements.

Advanced numerical methods suitable to simulate large deformations have been recently applied to simulate slope stability problems, such as, for instance, the Smoothed Particle Hydrodynamics (SPH) (e.g. Bui and Fukagawa 2013, Pastor et al. 2009), the Particle Finite Element Method (PFEM) (Zhang et al. 2015) and the Material Point Method (MPM) (Soga et al. 2016).

In this study a fully coupled MPM approach for unsaturated soil (Ceccato et al. 2019), whose description is provided in Section 3, is used to simulate the whole landslide process up to the determination of run-out distances and velocities of the original ski slope. It is shown that MPM is an effective and suitable tool to simulate the whole failure process if the slope geometry, soil hydro-mechanical properties and boundary conditions can be defined in a reasonably accurate way.

2 GEOLOGICAL AND GEOTECHNICAL SETTINGS

From a geological point of view, the landslide area lies at the border between the crystalline (Bressanone Phyllites) and sedimentary (Val Gardena sandstone) bedrock, followed by the Bellerophon Formation. Figure 2 depicts a cross section of the slope with soil and rock profile. This has been sketched from several seismic geophysical investigations together with 5 boreholes driven up to the deep intact sandstone bedrock.

Comparing the profiles before and after the mass collapse, it can be noted that the flow slide involved the detrital cover and partially the fractured and altered sandstone, sliding on thin layers of clayey-silt material lying at depths 5-20 m and gently sloping towards the valley.

Laboratory determination of Atterberg limits are $w_L = 18 - 28\%$, $w_P = 13 - 18\%$ with natural water content in the range $w_0 = 5 - 17\%$, suggesting that these fine layers are stiff overconsolidated clayey silts.

In absence of undisturbed samples (due to the presence of compacted fine soil matrix with some small lithic elements), the shear strength has been measured using direct shear tests carried out on reconstituted samples on soil passing to 2 mm sieve. To measure residual strength, direct shear tests have been performed on specimens in which a failure surface was created using the reversal procedure. Fig-

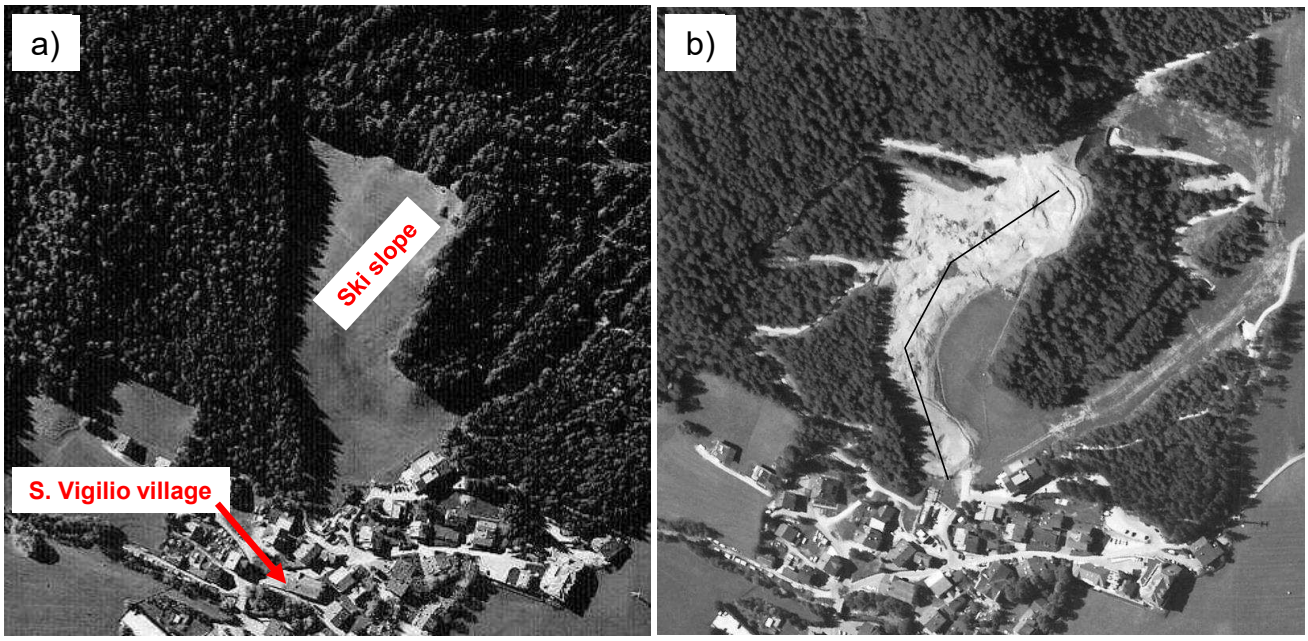

Figure 1: Aerial views of Cianross slope: a) before and b) after the collapse event (black line indicate the reference section shown in Fig. 2).

ure 3 shows the results of shear strength determination in 26 direct shear tests, together with the failure criterion used in MPM simulations.

3 TWO-PHASE MPM FORMULATION FOR UNSATURATED SOIL

MPM is a continuum-based method that applies two levels of spatial discretization: (i) the body is discretized by a cloud of material points (MPs), which move attached to the material and carry all the updated information such as velocities, strain, stresses, and history variables; and (ii) a fixed finite element mesh used to assemble and solve the system of equilibrium equations. Large deformations are simulated by MPs moving through the computational nodal grid that covers the full problem domain (Sulsky et al. 1994).

At the beginning of each time increment, the information is mapped from the MPs to the computational nodes of the mesh by means of the interpolation functions (Fig. 4a). The governing equations of motion are solved (Fig. 4b) and the nodal values are used to update the velocity, the position and to compute strains and stresses at the MP (Fig. 4c). At the end of the time step, the mesh may be changed arbitrarily, but it is usually kept fix. The assignment of MP to finite elements is updated after mesh adjustment (Fig. 4d).

The applied software, Anura3D (www.Anura3D.eu), implements an enhanced version of the original MPM, which has been extensively validated for geomechanical problems, see e.g. Ceccato et al. (2016), Jassim et al. (2013), Yerro et al. (2015).

Soil is a mixture of solid grains, and fluids like water and air filling the voids. The interaction between these phases determines the mechanical response of the material. The governing equations of the problem are the dynamic momentum balances of the liquid phase (Eq. 1) and the mixture (Eq. 2), the solid and liquid mass balances (Eq. 3 and 4), and the constitutive relationships. The subscript S and L indicate that the quantity refers to the solid or liquid respectively, ρ=density, $\rho_m = (1-n)\rho_S + nS_L\rho_L$=mixture density, n=porosity, p_L= pressure, σ=total stress, S_L= degree of saturation.

$$\rho_L \mathbf{a_L} = \nabla p_L - \mathbf{f^d} + \rho_L \mathbf{g} \tag{1}$$

$$(1-n)\rho_S \mathbf{a_S} + nS_L\rho_L \mathbf{a_L} = \nabla \cdot \sigma + \rho_m \mathbf{g} \tag{2}$$

$$\frac{Dn}{Dt} = n\nabla \cdot \mathbf{v_S} \tag{3}$$

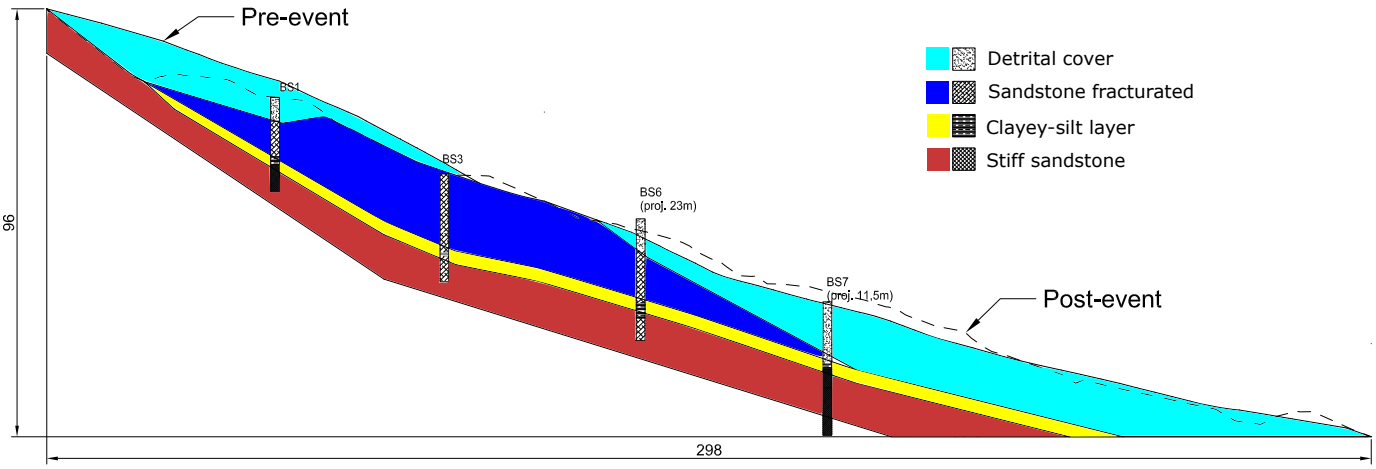

Figure 2: Stratigraphy of the cross section indicated with black line in Figure 1.

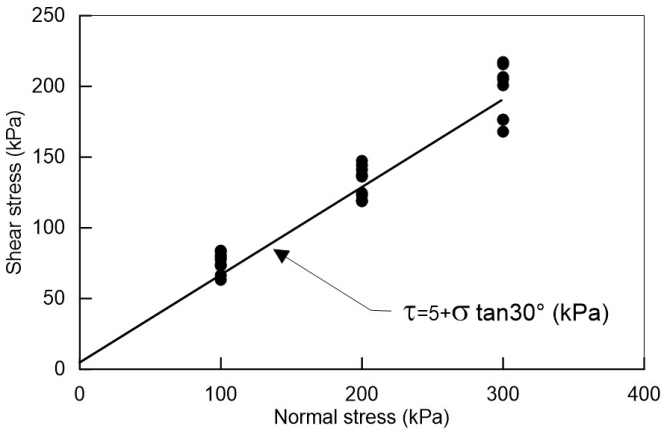

Figure 3: Results of direct shear test and estimate of friction angle for clayey-silt material.

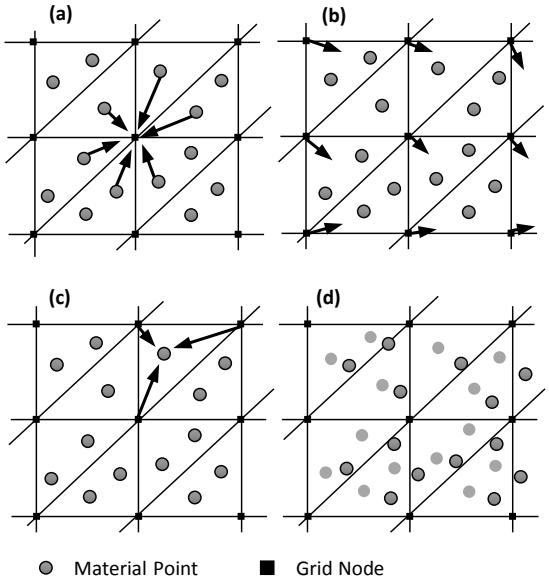

Figure 4: Computation scheme of MPM: a) map information to the nodes, (b) solve the governing equations of motions at the nodes, (c) update MP quantities (d) update MP housekeeping.

$$\left[-\frac{nS_L}{K_L}+n\frac{\partial S_L}{\partial p_L}\right]\frac{Dp_L}{Dt}=$$

$$nS_L\nabla\cdot\mathbf{v_L}+(1-n)S_L\nabla\cdot\mathbf{v_S} \quad (4)$$

In Eq. 1 and 2 partial saturation is accounted by means of the degree of saturation S_L. All dynamic terms are taken into account, and the accelerations a_S and a_L are the primary unknowns. These equations are discretized in space with the Galerking procedure and solved explicitly in time.

Solid and liquid mass balances (Eq. 3 and 4), as well as constitutive relationships are solved at the MPs.

The drag force $\mathbf{f^d}$ is linearly dependent on relative velocity $(\mathbf{v_L}-\mathbf{v_S})$ (Darcys law, eq. 5) and it accounts for the variations of the degree of saturation S_L. k_L is the hydraulic conductivity which is a function of the degree of saturation.

$$\mathbf{f^d}=\frac{n^2S_L\rho_Lg}{k_L(S_L)}(\mathbf{v_L}-\mathbf{v_S}) \quad (5)$$

The degree of saturation varies as a function of suction, and the well know Van Genuchten soil-water retention curve (SWRC) (Van Genuchten 1980) can be used with assumed constant parameters λ and p_0 (Eq. 6).

$$S_L=S_{min}+$$

$$\left[1+\left(\frac{s}{p_0}\right)^{\frac{1}{1-\lambda}}\right]^{(-\lambda)}(S_{max}-S_{min}) \quad (6)$$

The MPM solution scheme for each time step can be summarized as follow:

- Liquid nodal acceleration $\mathbf{a_L}$ is calculated by solving the discretized form of Eq. 1
- $\mathbf{a_L}$ is subsequently used to obtain the nodal acceleration of the solid $\mathbf{a_s}$ from the discretized form of Eq. 2.
- Velocities and momentum of the MPs are updated from nodal accelerations of each phase.
- Nodal velocities are then calculated from nodal momentum and used to compute the strain rate at the MP location.
- Eq. 3 and 4, together with the constitutive laws, give the increment of excess pore pressure and effective stress.
- Degree of saturation and hydraulic conductivity are updated considering SWR and hydraulic conductivity curves.
- Displacement and position of each MP is updated according to the velocity of the solid phase.

4 NUMERICAL MODEL

Cianross slope collapse is analyzed with a 2D plane strain numerical model. The reference section is shown in Figure 5; the model is 315m-wide and 115m-high. The model spatial discretization consists in an unstructured mesh of 1954 triangular elements, specially refined in correspondence of the three upper layers. Three material points are initially positioned inside each active element forming the slope.

In agreement with the geotechnical surveys interpretations, the stratigraphy considers four different materials: a detrital cover on the top, followed by a fractured sandstone (Arenaria della Val Gardena) and a thin clayey-silt layer which represents the weakness plane of the entire slope. Below, a compact sandstone layer is present up to significant depth, but for computational purpose it is reduced to a limited thickness (approximately 10 m).

Taking in account previous geological and geotechnical considerations about the site conditions and resistance properties among various banks, the three upper layers are modelled with an elastic-perfectly plastic Mohr-Coulomb model, while the stiffer compact sandstone is assumed linear elastic. Elastic parameters are the same for all the materials and are lower than real in order to reduce the computational cost, i.e. Young modulus $E = 20 \cdot 10^3$ kPa and Poisson ratio ν = 0.3; whereas friction angles ϕ and cohesion values c', summarized in Table 1, are selected in accordance with the ranges resulting from geotechnical lab tests.

Table 1: Mechanical parameters of the layers modelled with Mohr-Coulomb

Material	$\phi\,[^\circ]$	$c'\,[kPa]$
Fracturated sandstone	33	5
Detrital cover	30	3
Clayey-silt	30	5

Table 2: Water parameters

Parameter	value
Density [kg/m^3]	1000
Bulk modulus [kPa]	$80{\cdot}10^3$
Dynamic viscosity [kPa $\cdot$ s]	10^{-6}

The initial porosity is taken equal to 0.4 for all the materials and solid density ranges between 2650 and 2700 kN/m^3. In this study a two-phase approach is adopted to reproduce soil behavior interacting with water, thus the parameters of this last need to be defined, together with "interaction" parameters between phases. In table 2 water parameters are reported and a reduced value of water bulk modulus is adopted for computational efficiency.

Concerning the partially saturated behavior of the soil, the Van Genuchten hydraulic model is used. Since, no laboratory specific tests were available to make an estimation of the Van Genuchten parameters, typical values for the type of materials found in the field are used. The soil water retention curve is given in Eq. (6) with parameters $S_{max} = 1$, $S_{min} = 0.025$, $p_0 = 6\,kPa$, $\lambda = 0.07$.

The hydraulic conductivity $4.9 \cdot 10^{-3}$ m/s is used to model infiltration and flow process occurring in the slope. This value is higher than real permeability, but it ensures reduced simulation times and satisfactory physical results, adhering to the phenomena we aimed to reproduce.

With the aim of reproducing the complex sequence of events occurred at Cianross ski slope causing the collapse, the numerical simulation is subdivided in three stages:

A. Stress initialization in quasi static conditions: starting from the knowledge of water levels from the monitoring system installed after the collapse, it was possible to derive the potential position of the water table before the landslide.

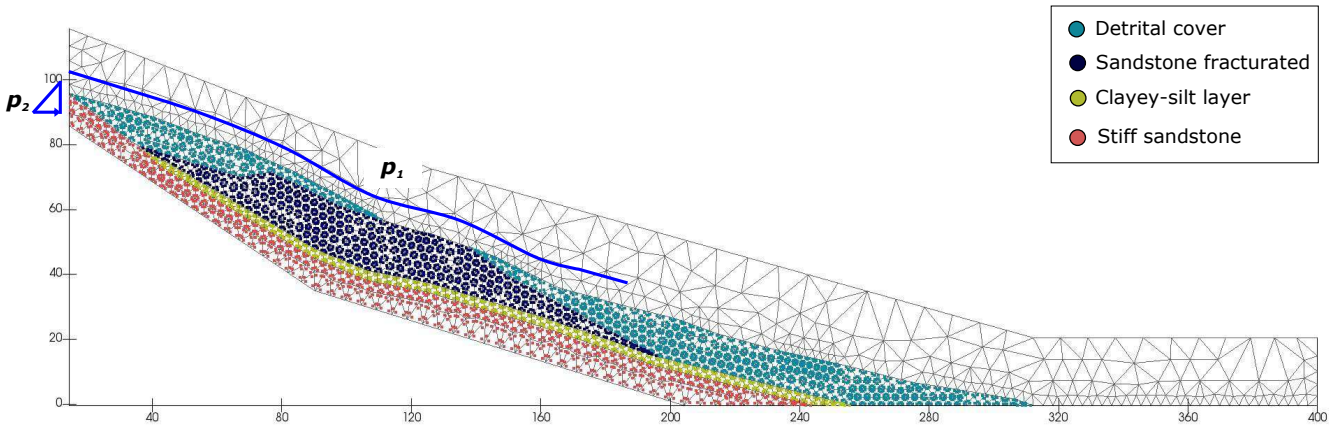

Figure 5: MPM model of Cianross ski slope. Background computational mesh, MPs discretization, materials and hydraulic boundary conditions are depicted.

This last is taken as the preexisting initial condition for pressure distribution in the slope, and accordingly, a suction $p_1 = 100kPa$ is applied at the surface of the slope, up to the location of the spring emergence in the lower part. In this manner, the condition of partial saturation of the slope's upper portion is effectively reproduced. Furthermore, to overcome the computational difficulty of initializing stress for both the phases, firstly the solid skeleton is kept undeformable to allow pore pressure distribution. Subsequently, the soil deformability is introduced and cohesion values assumes an artificial high value, equal to 100 kPa, to avoid problems of model rebound induced by the sudden application of gravity. Finally, cohesion values are reduced to their actual values, as presented in table 1, and the slope reaches an equilibrium state under the boundary conditions and acting forces.

B. Melting snow infiltrating: to mimic this process, with a potential contribution to Cianross slope instability, the applied suction value of 100 kPa at the slope top is suddenly removed, thus turning the pressure condition to 0 kPa. This phase can be interpreted as the onset of the dynamic process, causing a consistent reduction of the effective stress state.

C. The rupture of the snow gun pipeline system on the slope upper portion resulting in additional saturation: this occurrence, identified as the second major responsible of the landslip, is simulated by means of a hydrostatic gradient of pressure at the lateral vertical boundary of the slope, i.e. close to the real location of the pipeline.The sudden application of this negative pressure, together with the continuous progression of the upper infiltration, generated the full saturation of at least the upper layers, followed by the collapse and the propagation of a slurry flow till the village immediately near the slope foot. This process is tracked for a simulation time of 900 s.

In the following section the overall analysis of the numerical results and the comparison with the real profile data will be presented.

5 RESULTS

The applied 2-phase formulation with suction allows to track saturation degree's evolution with the acting pore pressures and simultaneously to observe the onset of motion and its entire evolution, i.e. the complete post-failure behavior.

In the present study, the method reveals its potentiality in slope stability risk assessment, where a deeper understanding of the mobilizing sequence was required. First, a normalized time is defined as a reference for the simulation time scale (Ceccato et al. 2019, Alonso and Lloret 1983). The dimensionless time is defined as

$$T = \frac{C_i t}{h^2} \tag{7}$$

where t [s] is the simulation time, h [m] is the thickness of the drainage path, thus in the present case is take approximately equal to 15 m, considering the infiltration process in the upper three layers. The infiltration coefficient C_i [m^2/s], similar to the consolidation coefficient, assumes the following expression:

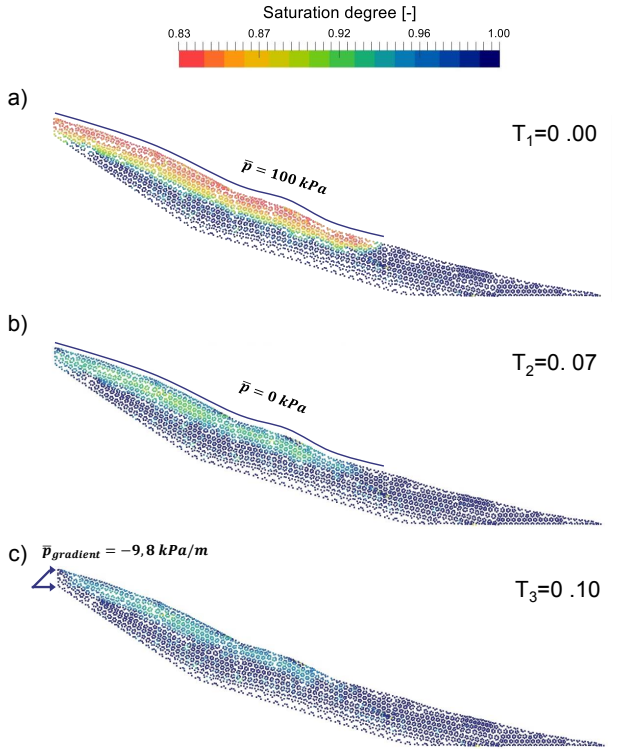

Figure 6: Contour of saturation degree S_L. a) Initial state, b) onset of snow infiltration and d) pipe line rupture at slope top.

$$C_i = \frac{k}{n\rho_l g(\frac{S_L}{K_L} + a_s)} \tag{8}$$

where a_s=0.0033 [1/kPa] is the slope of the linear function approximating the S_L expression in the range of values reached during the simulation. Therefore, the final expression of the normalized time is:

$$T = (1.6771 \cdot 10^{-3})t \tag{9}$$

The immediate result of the pore pressure distribution, generated by local alterations, is the variation of saturation degree, as presented in Figure 6. To appreciate the differences, three significant moments of the simulation process are reported: a) at the beginning of the simulation ($t_1 = 0$), after stress initialization; b) immediately after removal of the superficial pressure condition ($t_2 = 0.07$) and c) right after application of the lateral gradient of pressure ($t_3 = 0.10$). S_L contour in Figure 6a is a direct consequence of the assumed pressure boundary condition, which guarantees to reproduce a specific initial condition in accordance with the piezometers data, showing water table location ordinarily between 10 and 15 m depth.

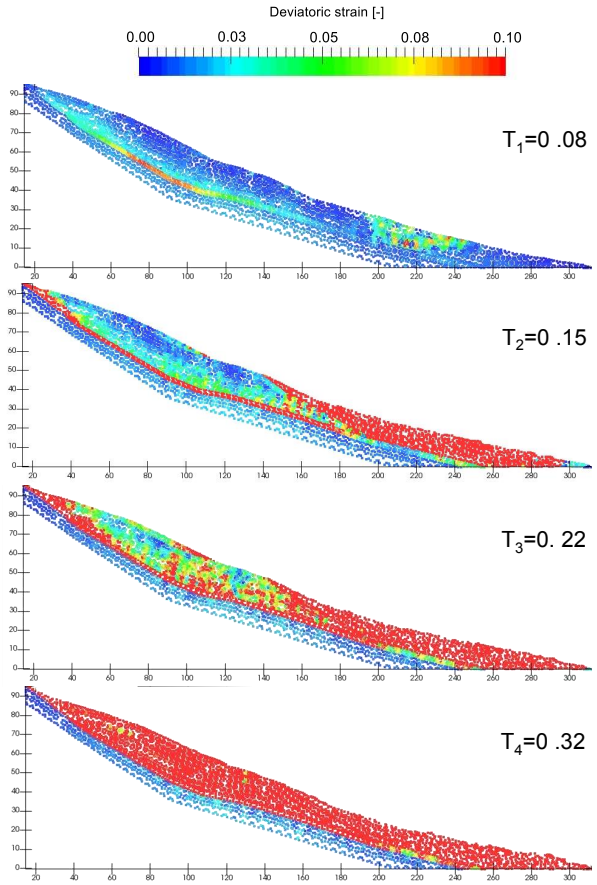

Figure 7: Evolution of deviatoric strain plotted at normalized time instants.

Figure 7 shows the evolution of deviatoric strain in four progressive normalized time instants: in the first picture it is immediately evident the localization along the clayey-silt layer, followed by the instability of the lower saturated portion of the slope. This last, composed by the detrital soil cover, is also characterized by the more unfavorable combination of cohesion and friction angle values, thus the onset of motion is coherently localized there. In the subsequent two time instants, pictures show the retrogressive character of the sliding mechanism, where the plasticized zones increase progressively towards the slope head. In particular, the fractured sandstone is the layer which lastly accumulate strains and displaces, confined between the fill portions undergoing extension, firstly at the foot and then on the top.

In order to assess the influence of the pore pressure upsurge due to pipeline rupture, a simulation without stage C (additional pore pressure as explained in Sec. 4) is performed. Figure 8 compares the final displacement obtained without the lateral gradient of pressure (contour a) with the reference case with the lateral pressure applied (contour b). The in-situ estimate of the initial slope profile (green line) and the final profile after collapse

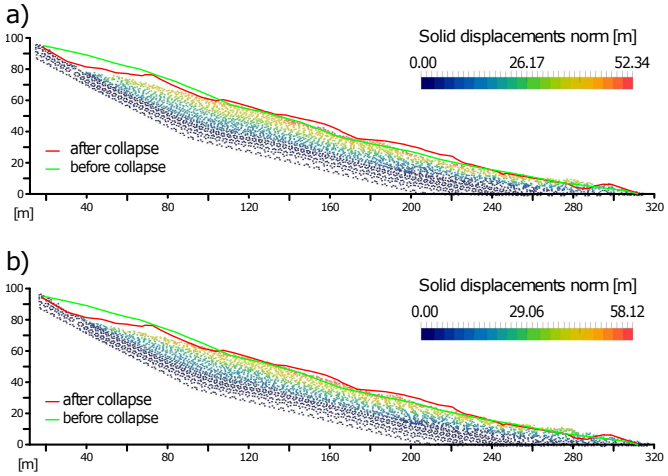

Figure 8: Displacements contour at normalized t= 1.58, compared with detected initial and final slope profiles. Case a) in absence of hydraulic load on the top, case b) with the hydraulic load.

(red line) are are shown.

Case b) shows displacements approximately 10% larger then case a), however the overall results indicate that the deformed shape is similar. Case b) profile seems to be positioned closer to the real final profile, especially in the central portion of the slope, between 100 and 220 m referring to the horizontal scale of Figure 8. Material points locations for both the cases resemble the real profile in the previously mentioned central portion until x=260 m, whereas the upper part tends to be in a lower position, relative to the real profile, and the foot shows a slightly bigger amount of accumulated material.

6 CONCLUSIONS

This paper presented a ski-slope failure and the subsequent run-out due to reactivation of pre-existing small quiescent landslide by water infiltration due to snow melting and snow gun pipeline rupture, that saturated the shallow detrital cover. The case study is simulated with a fully coupled 2-phase MPM formulation able to capture the hydromechanical behaviour of unsaturated soil from the one-set of failure to landslide deposition. Despite the relatively simple hydromechanical hypothesis to characterize the soil and rock formation, preliminary results show a good agreement with field observations in predicting such a complex sliding and fluidization phenomenon. Further improvements can be obtained considering the three-dimensional effects and more advanced soil constituive models.

REFERENCES

Alonso, E. E. & A. Lloret (1983). Evolution in time of the reliability of slopes in partially saturated soils. In Pitagora (Ed.), *Applications of Statistics and Probability in Soil and Structural Engineering*, Firenze, pp. 1363–1376.

Bui, H. & R. Fukagawa (2013). An improved SPH method for saturated soils and its application to investigate the mechanisms of embankment failure: Case of hydrostatic porewater pressure. *International for Numerical and Analytical Methods in Geomechanics 37*(October 2011), 31–50.

Ceccato, F., L. Beuth, & P. Simonini (2016). Analysis of Piezocone Penetration under Different Drainage Conditions with the Two-Phase Material Point Method. *Journal of Geotechnical and Geoenvironmental Engineering 142*(12), 4016066.

Ceccato, F., V. Girardi, & P. Simonini (2019). Developing and testing multiphase MPM approaches for the stability of dams and river embankments. In *AIMETA 2019*, Number September, Rome, pp. 15–19.

Ceccato, F., V. Girardi, A. Yerro, & P. Simonini (2019). Evaluation of dynamic explicit MPM formulations for unsaturated soils. In E. Oñate, M. Bischoff, D. Owen, P. Wriggers, and T. Zohdi (Eds.), *Particles 2019*, Barcellona.

Jassim, I., D. Stolle, & P. Vermeer (2013). Two-phase dynamic analysis by material point method. *International Journal for Numerical and Analytical Methods in Geomechanicsnumerical and analytical methods in Geomechanics 37*, 2502–2522.

Pastor, M., B. Haddad, G. Sorbino, S. Cuomo, & V. Drempetic (2009). A depthintegrated, coupled SPH model for flowlike landslides and related phenomena. *International Journal for Numerical and Analytical Methods in Geomechanics 33*(2), 143–172.

Soga, K., E. Alonso, A. Yerro, K. Kumar, & S. Bandara (2016). Trends in large-deformation analysis of landslide mass movements with particular emphasis on the material point method. *Géotechnique 66*(3), 248–273.

Sulsky, D., Z. Chen, & H. Schreyer (1994). A particle method for hystory-dependent materials. *Computer Methods in Applied Mechanics and Engineering 118*(1-2), 179–196.

Van Genuchten, M. (1980). A closed-form equation for predicting the hydraulic conductivity of unsaturated soils. *Soil science society of America journal 44*(5), 892–898.

Yerro, A., E. Alonso, & N. Pinyol (2015). The material point method for unsaturated soils. *Geotechnique 65*(3), 201–217.

Zhang, X., K. Krabbenhoft, D. Sheng, & W. Li (2015). Numerical simulation of a flow-like landslide using the particle finite element method. *Computational Mechanics 55*(1), 167–177.